Ferroelastic strain control of multiple nonvolatile resistance tuning in $SrRuO_3$/PMN-PT(111) multiferroic heterostructures

Ming Zheng,[1,a)] Hao Ni,[1,2] Yaping Qi,[1] Weiyi Huang,[1] Jiali Zeng,[1] and Ju Gao[1,a)]
[1]*Department of Physics, The University of Hong Kong, Pokfulam Road, Hong Kong*
[2] *College of Science, China University of Petroleum, Qingdao 255680, China*

(Received 9 April 2017; accepted 21 April 2017; published online 2 May 2017)

The electric-field-tunable resistance switching in elastically coupled $SrRuO_3$ thin films grown on (111)-oriented $0.7Pb(Mg_{1/3}Nb_{2/3})O_3$-$0.3PbTiO_3$ ferroelectric-crystal substrates has been investigated. During the ferroelectric poling process, the resistance evolution tracks the electric-field-induced in-plane strain of the film efficiently, revealing strain but not the electrostatic charge-mediated coupling mechanism. Using 109° and 71° ferroelastic domain switching of the substrate, multiple reversible and nonvolatile resistance states can be achieved at room temperature, which is closely related to the relative proportion of in-plane polarization vectors and induced distinct in-plane strain states after domain switching. Our findings provide an approach to elucidate electrically driven domain switching dynamics and design energy efficient, high-density spintronic memory devices. *Published by AIP Publishing*. [http://dx.doi.org/10.1063/1.4983018]

A central challenge in altering the magnetic and electronic phases in correlated oxide systems lies in finding an energy efficient way to collect reversible and nonvolatile states by voltage control, due to their promising applications in next-generation nonvolatile hybrid spintronic devices.[1–6] Among the popularly known correlated oxides, ferromagnetic metal $SrRuO_3$ (SRO) has attracted ever-increasing attention for decades due to its striking magnetic and electrical properties such as exchange bias,[7] vertical hysteretic shifts,[8] magnetocrystalline anisotropy,[9] and anomalous Hall effects[10] and for its potential applications in spin valves, magnetic recording media, and magnetic tunnel junctions.[11] It is well-known that multiferroic heterostructures composed of ferromagnetic and ferroelectric layers have been extended as a knob to *in situ* manipulate charge and/or the lattice-coupled physical properties of the ferromagnetic layer by using a voltage across the ferroelectric layer due to the strong magnetoelectric coupling effect. For example, Ahn *et al.*[12,13] observed 9% change in resistance through the voltage induced charge accumulation/dissipation at the interface of the SRO/$Pb(Zr_{0.52}Ti_{0.48})O_3$ heterostructure, whereas the SRO film is required to be ultrathin (30 Å thick) due to an infinitesimal Debye screening length. Additionally, Herklotz *et al.*[14] and Zhou *et al.*[15] *in situ* applied in-plane compressive strains to SRO films grown on the $Pb(Mg_{1/3}Nb_{2/3})O_3$-$PbTiO_3$ (PMN-PT) ferroelectric substrates using piezo responses and realized strain-mediated voltage control of magnetic and transport properties. However, the lattice strain states produced by the linear converse piezoelectric effect cannot retain upon removal of the driving voltage, and thus, the modulation of physical properties is volatile. Fortunately, several exceptions have been reported, e.g., on $Co_{40}Fe_{40}B_{20}$/PMN-PT(001),[16] $Fe_{60}Co_{20}B_{20}$/PMN-PT(011),[17] Fe_3O_4/PMN-PT(011),[18] VO_x/PMN-PT(011),[19] and $La_{2/3}Ba_{1/3}MnO_3$/PMN-PT(011)[20] heterostructures, and voltage-impulse-induced nonvolatile tuning of physical parameters including ferromagnetic resonance frequency and metal-insulator transition temperature can be achieved using non-linear lattice strain effects originating from the non-180° ferroelectric polarization reorientation. There is no doubt that an in-depth understanding of electrically driven domain switching dynamics and selective control of the polarization switching pathway will help to obtain electrically tunable nonvolatile switching of lattice-sensitive order parameters in a stable and reversible manner, which is also indispensable from a device application point of view.

In this work, we fabricated epitaxial SRO thin films on (111)-oriented $0.7Pb(Mg_{1/3}Nb_{2/3})O_3$–$0.3PbTiO_3$ (PMN-PT) ferroelectric single-crystal substrates. A unique ferroelastic switching (109° and 71°) pathway in PMN-PT(111) was exploited to produce distinct lattice strain states by rotating the polarization vectors between the out-of-plane and in-plane directions by reversing an electric field with appropriate magnitude (less than the coercive field of PMN-PT). Using this reversible ferroelastic strain effects, multiple stable nonvolatile resistance states can be generated at room temperature. Our approach offers an energy efficient way to design prototype devices for nonvolatile information storage.

SRO films (~28 nm thick) were prepared on (111)-oriented PMN-PT single-crystal substrates by pulsed laser deposition. The growth was carried out under 15 Pa oxygen pressure at 700 °C, followed by *in situ* annealing in 1 atm O_2 for 30 min to reduce oxygen deficiencies and to improve crystallinity. The film crystal structure was characterized using a high resolution Bruker D8 Discover X-ray diffractometer (XRD) attached with a Cu $K_{\alpha 1}$ radiation source ($\lambda = 1.5406$ Å). Figure 1(a) illustrates the schematic of the experimental setups for *in situ* measurements of resistance (using the standard four-probe method) and out-of-plane strain of SRO films (using *in situ* XRD θ-2θ scans). The electric-field-induced in-plane strain of the PMN-PT substrate was measured using a strain gauge bonded on the substrate surface with epoxy [see Fig. 1(b)]. The ferroelectric domain switching and ferroelastic domain switching were

a)Authors to whom correspondence should be addressed. Electronic addresses: zhengm@mail.ustc.edu.cn and jugao@hku.hk

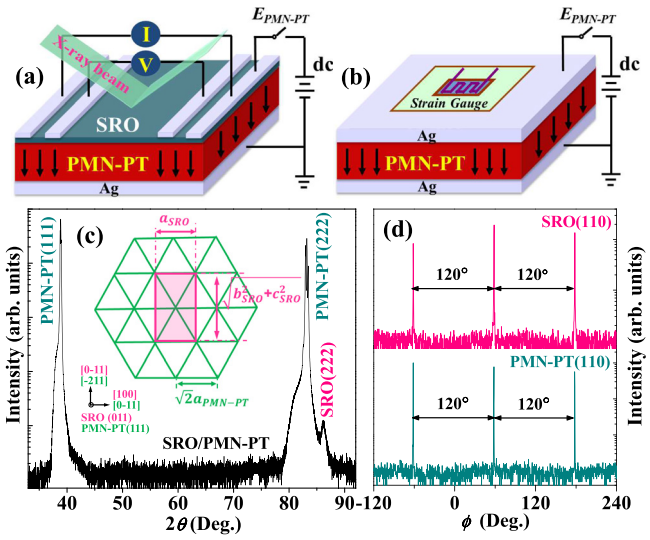

FIG. 1. Schematic of the experimental setups for *in situ* measurements of film resistance, out-of-plane strain (a) and in-plane strain (b) of the PMN-PT substrate, respectively. (c) XRD θ-2θ scan of the SRO/PMN-PT structure. The inset shows a schematic of in-plane lattice arrangements for the orthorhombic SRO unit cell on the PMN-PT(111) substrate. (d) XRD ϕ scans taken on the SRO(110) and PMN-PT(110) diffraction peaks.

conducted by vertically applying a dc electric field across the PMN-PT substrate through the metallic SRO film and the thermal-evaporated bottom silver electrode. The domain switching dynamics at the surface of the PMN-PT substrate were analyzed by piezoresponse force microscopy (PFM).

Figure 1(c) presents the XRD θ-2θ scan pattern of the as-grown SRO/PMN-PT heterostructure. We found that the SRO film has no impurities and is highly (111)-oriented. The in-plane epitaxial relationship between the film and the substrate was assessed by performing XRD ϕ-scans, which were taken on the (110) diffraction peaks of the SRO film and the PMN-PT substrate, respectively. As depicted in Fig. 1(d), two sets of trifold symmetrical diffraction peaks recurring every 120° were observed at the same azimuthal ϕ angle, clearly signaling the good "cube-on-cube" epitaxial nature of the SRO film on the PMN-PT substrate. A schematic diagram of the in-plane lattice arrangements of the orthorhombic SRO unit cell on the pseudocubic PMN-PT substrate is shown in the inset of Fig. 1(c). The out-of-plane lattice spacing d_{111} of the SRO film (~2.256 Å) is smaller than that of the bulk value (~2.269 Å),[11] which means that the SRO film suffers an in-plane tensile strain and an out-of-plane compressive strain (-0.57%). This result is consistent with the smaller lattice parameters of the SRO bulk ($a \sim b \sim c \sim 3.93$ Å)[11] compared with those of the PMN-PT substrate ($a \sim b \sim c \sim 4.02$ Å).

The impact of electric-field-induced ferroelectric poling of the PMN-PT substrate on the electronic transport property of the SRO film is displayed in Fig. 2(a), where the electric-field-induced relative resistance variation $\Delta R/R$ follows the electric-field-induced out-of-plane tensile strain $\delta\varepsilon_{zz(SRO)}$ of

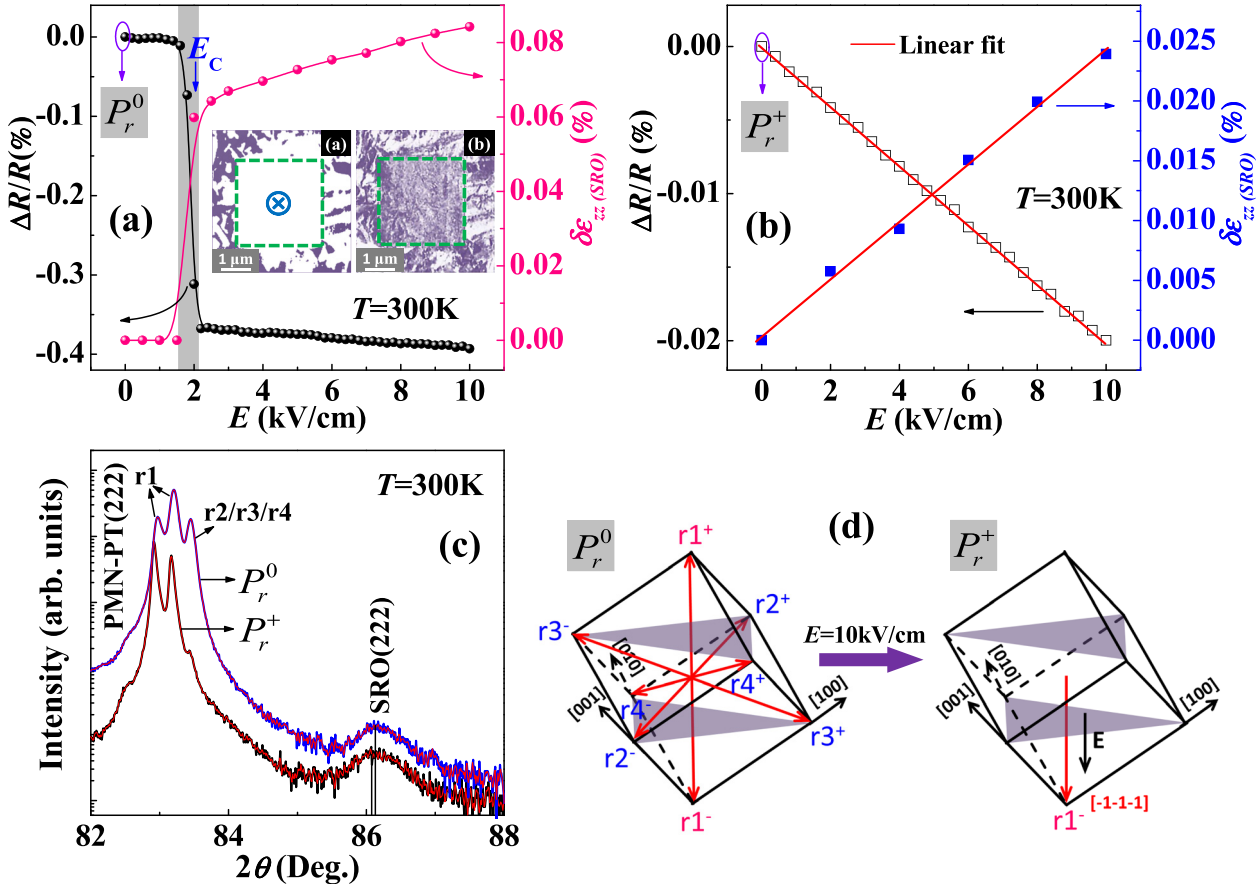

FIG. 2. (a) $\Delta R/R$ and electric-field-induced out-of-plane strain $\delta\varepsilon_{zz(SRO)}$ of the SRO films as a function of E. Insets (a) and (b) show the out-of-plane and in-plane PFM phase images of the PMN-PT substrate, respectively. (b) $\Delta R/R$ and $\delta\varepsilon_{zz(SRO)}$ as a function of positive E applied to the positively poled PMN-PT substrate. (c) XRD θ-2θ scans for the PMN-PT(222) substrate and the SRO(222) film under the P_r^0 and P_r^+ states, respectively. (d) Schematic of the polarization vectors in the rhombohedral phase under P_r^0 and P_r^+ states for the PMN-PT.

the film effectively during the poling process along the thickness direction. The nonlinear abrupt evolution in both film resistance and $\delta\varepsilon_{zz(SRO)}$ near E_C (~2.2 kV/cm) of the PMN-PT substrate discloses the intimate correlation between the electronic transport and the strain state of the film. We note that after applying a sufficiently large positive dc electric field (e.g., $E = 10$ kV/cm) across the SRO/PMN-PT heterostructure, both the PMN-PT(222) and SRO(222) diffraction peaks shift to lower 2θ angles as evidenced by *in situ* XRD measurements [see Fig. 2(c)], implying that in-plane (out-of-plane) lattices of both the PMN-PT and the SRO contract (expand) after positive poling. Previous experiments have demonstrated that the poling-induced remnant strain microscopically stems from the reorientation of ferroelectric domains in the PMN-PT single-crystal substrate.[16–20] Consequently, we measured the PFM phase images of the PMN-PT(111) substrate during domain switching and presented the results in the insets (a) and (b) of Fig. 2(a). As shown in Fig. 2(d), the eight spontaneous polarization vectors of the rhombohedral PMN-PT(111) crystal randomly point along the body diagonals of the pseudocubic cell in the initial or unpoled state (denoted by P_r^0), corresponding to four structural domains (r1, r2, r3, and r4) with a mixture of out-of-plane and in-plane polarization components [see insets (a) and (b) of Fig. 2(a)]. Upon applying a poling voltage of +8 V on the tip, the 180° ferroelectric switching (from $r1^+$ to $r1^-$), 109° ferroelastic switching (from $r2^+/r4^+/r3^-$ to $r1^-$), and 71° ferroelastic switching (from $r2^-/r4^-/r3^+$ to $r1^-$) take place, and thus, all the polarization vectors rotate downward in the poled area (green box), pointing along the [-1–1–1] direction with no in-plane component (denoted by the P_r^+ state) [see Fig. 2(d)]. This polarization switching pathway under the vertically applied voltage impulse can also be determined by *in situ* XRD measurements. As can be seen in Fig. 2(c), the PMN-PT(222) reflection changes from three peaks to two peaks after positive poling, where the peak corresponding to the r2/r3/r4 domain structures almost disappears, and the relative intensity of the peaks corresponding to the r1 domain structure increases remarkably. All these data explicitly establish the effectiveness of electrically tunable ferroelectric and ferroelastic domain switching whether for local regions (micrometer size) or whole area (millimeter size) of the sample.

To gain deeper insights into the interaction between the electronic transport and the lattice strain, we applied a positive electric field E to the positively poled (P_r^+) PMN-PT substrate at room temperature ($T = 300$ K) and simultaneously recorded the induced relative resistance change $\Delta R/R$ and out-of-plane tensile strain $\delta\varepsilon_{zz(SRO)}$ of the film in Fig. 2(b). One can see that $\Delta R/R$ decreases linearly with increasing E from 0 to 10 kV/cm, which could be attributed to the converse-piezoelectric-effect-induced linear contraction (expansion) of the film in-plane (out-of-plane) lattice rather than the domain switching mediation.[21] Due to the linear electric field dependence, $\Delta R/R$ and $\delta\varepsilon_{zz(SRO)}$ can be expressed as $\Delta R/R = -aE$ and $\delta\varepsilon_{zz(SRO)} = cE$, respectively. Here, a and c are constants. Using the Poisson relation $\delta\varepsilon_{zz} = -2\nu/(1-\nu)\delta\varepsilon_{xx}$,[22] where ν is the Poisson ratio, the quantitative relationship between the $\Delta R/R$ and the induced in-plane strain of the film can be obtained and expressed as $\Delta R/R = (a/c)(2\nu/1-\nu)\delta\varepsilon_{xx(SRO)}$. This resistance-strain relationship proves that the relative resistance evolution in the SRO film is proportional to the induced in-plane compressive strain in the film.

Figure 3(a) shows the resistance of the SRO film in response to the *in situ* electric field with different switching pathways at room temperature. Upon cycling a large bipolar electric field with an amplitude of $E = 8$ kV/cm, the film resistance exhibits a butterfly-like loop with respect to the electric field (cyan curve). Nevertheless, when cycling a small unipolar electric field [e.g., $E = 2$ kV/cm$<E_{C(PMN-PT)}$], a hysteresis-like loop of $(\Delta R/R)_{strain}$ to E was observed (peak

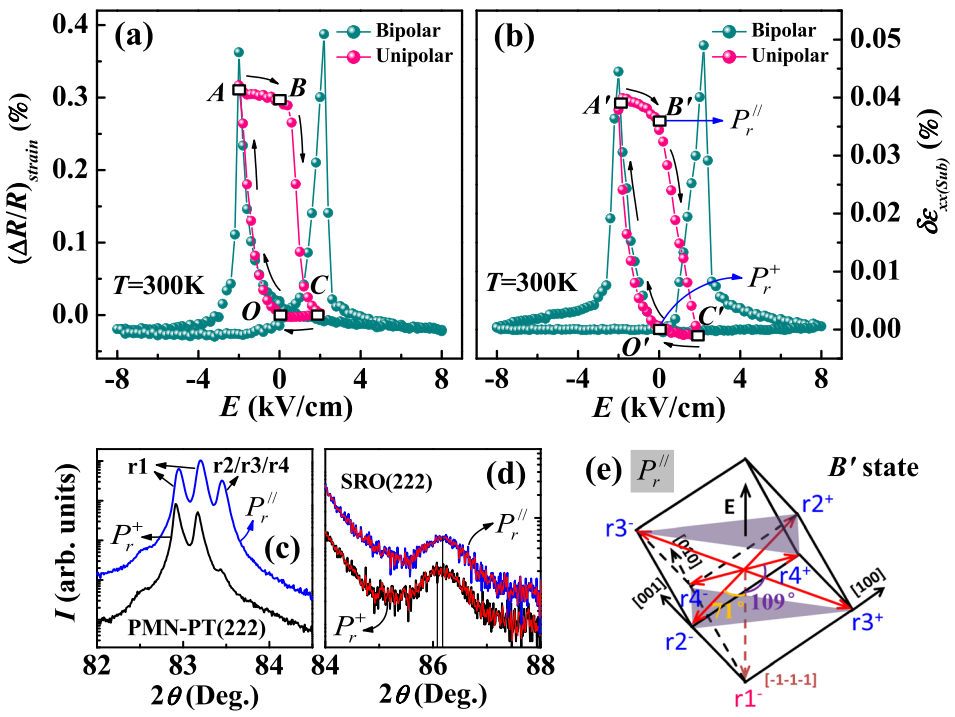

FIG. 3. Electric-field-induced relative resistance evolution (a) of the SRO film and in-plane strain (b) of the PMN-PT substrate as a function of bipolar and unipolar E applied across PMN-PT at $T = 300$ K. (c) and (d) XRD θ-2θ scans for the PMN-PT(222) substrate and the SRO(222) film under P_r^+ and $P_r^{//}$ states, respectively. (e) Schematic of the polarization vectors in the rhombohedral phase from the P_r^+ state to the $P_r^{//}$ state for the PMN-PT.

curve). Here, $(\Delta R/R)_{strain}$ is defined as $(\Delta R/R)_{strain} = [R(\mathrm{E}) - R(P_r^+)]/R(P_r^+)$. In-plane strain measurements [see Fig. 3(b)] reveal that the electric-field-induced in-plane strain curves ($\delta\varepsilon_{xx(Sub)}$ versus E) of the PMN-PT substrate have similar patterns (butterfly-like or hysteresis-like loops) as those of the resistance curves ($(\Delta R/R)_{strain}$ versus E) of the SRO film whether by sweeping bipolar or unipolar electric fields. This finding provides the direct evidence of the strain-induced nature of the resistance modulation. Considering the infinitesimal screening length (1–2 Å) of the electron in SRO films,[12] it is reasonable to preclude the electrostatic charge-mediated coupling mechanism in our 28 nm-thick SRO film. Notably, once applying a small negative electric field of $E=-2$ kV/cm [$|E|<E_{C(PMN-PT)}$] to the positively poled (P_r^+) PMN-PT substrate (i.e., ***O'*** state), the polarization switching pathways include 109° ferroelastic switching from r1$^-$ to r2$^+$/r4$^+$/r3$^-$ and 71° ferroelastic switching from r1$^-$ to r2$^-$/r4$^-$/r3$^+$ [see Fig. 3(e)], giving rise to the polarization vectors switching from the downward to the in-plane direction (denoted by $P_r^{//}$). In this scenario, an in-plan tensile strain (corresponding to ***B'*** state) was produced after the removal of the control voltage due to the stability of the remnant in-plane polarization of PMN-PT(111). Accordingly, the film resistance evolves from ***O*** to ***A*** then to the ***B*** state ($(\Delta R/R)_{strain}$~0.3%). *In situ* XRD measurements were performed to further investigate the structural evolution of the SRO/PMN-PT heterostructure during domain switching. As shown in Figs. 3(c) and 3(d), upon the polarization, the direction was rotated from the P_r^+ state to the $P_r^{//}$ state, and the PMN-PT(222) reflection splits from two peaks to three peaks. The relative intensity of the peaks corresponding to the r1 domain structure decreases considerably and the peak corresponding to the r2/r3/r4 domain structures reappears, directly confirming the above-mentioned 109° and 71° ferroelastic switching pathways. Moreover, both the PMN-PT(222) and SRO(222) diffraction peaks shift to higher Bragg angles upon polarization switching, suggesting an out-of-plane lattice contraction accompanied by an effective in-plane lattice expansion of both the PMN-PT and the SRO. We calculated the decreased out-of-plane compressive strain in the SRO film as 0.06%. According to the Poisson relation $\delta\varepsilon_{zz} = -2\nu/(1-\nu)\delta\varepsilon_{xx}$ and $\nu = 0.28$,[14] the increased in-plane tensile strain is estimated to be 0.077%. Therefore, the room temperature gauge factor β [$\beta=(\Delta R/R)_{strain}/\delta\varepsilon_{xx(SRO)}$] is calculated to be 390%, which is comparable to the value of the $CaMnO_3$/PMN-PT structure[23] for which there is also no Jahn-Teller distortion of BO_6 octahedra. The observed in-plane tensile strain induced enhancement of the film resistance can be explained in terms of stain-induced reduction in the orbital overlap between the Ru 4*d* orbitals and O 2*p* orbitals by adjusting the octahedral rotations.[24,25] The weakened orbital hybridization narrows the one electron bandwidth and thus enhances the electron correlation effect, thereby increasing the film resistance. Afterwards, by applying positive $E=+2$ kV/cm to the metastable PMN-PT substrate (i.e., $P_r^{//}$ state), the in-plane polarization of the substrate was switched back to the downward direction (i.e., the P_r^+ state). The film strain and resistance can also recover to the initial ***O'*** and ***O*** states, respectively, once the applied voltage is switched off. It is thus speculated that these two stable and switchable remnant strain (***O'*** and ***B'***) states will facilitate realizing nonvolatile resistance tuning by reversing the control voltage in the vicinity of $E_{C(PMN-PT)}$ in this system.

Aside from the resistance switching between the ***O*** and ***B*** states, any intermediate resistance state between them is reachable by precisely adjusting the amplitude of sweeping electric fields [see Fig. 4(a)], which could be linked by different remnant in-plane strain states of the substrate.[17,20,26,27] From the inset of Fig. 4(a), as the amplitude of the sweeping electric field is decreased from $E=2.0$ kV/cm to 0.8 kV/cm, the relative intensity of the peak corresponding to the r2/r3/r4 domain structures is reduced significantly but not to zero, indicating that the corresponding 109° ferroelastic switching from r1$^-$ to r2$^+$/r4$^+$/r3$^-$ and 71° ferroelastic switching from r1$^-$ to r2$^-$/r4$^-$/r3$^+$ become weakened gradually. Obviously, the relative proportion of in-plane polarization vectors switched from the [-1-1-1] direction is reduced, leading to the decrease in the remnant in-plane tensile strain of PMN-PT(111). Therefore, the multiple stable resistance states indeed arise from ferroelastic domain switching-induced distinct remnant strain states of the substrate. Based on Fig. 4(a), we construct ferroelastic-strain driven five reversible and nonvolatile resistance states ("0" to "4" states) by applying appropriate electric field pulses to the device, as shown

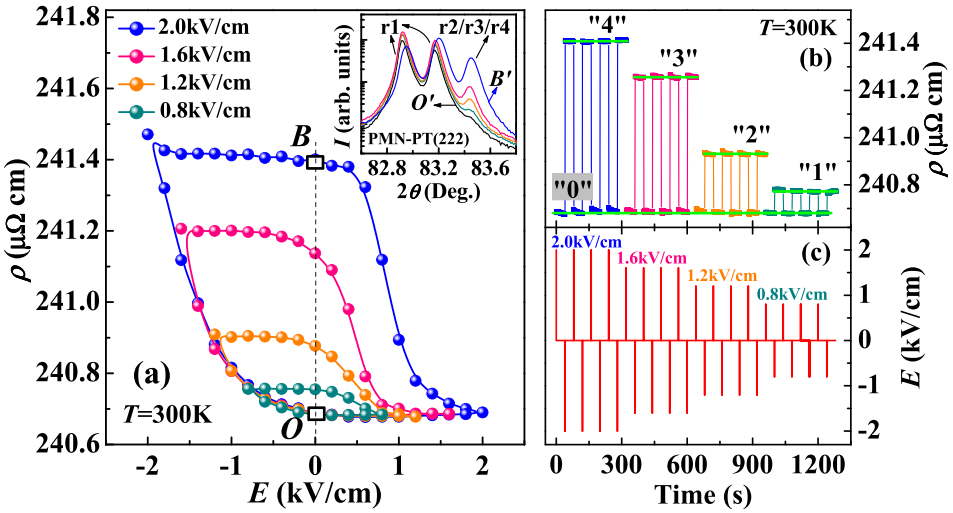

FIG. 4. (a) Resistance hysteresis loops with different amplitudes of the sweeping electric field as stated. The inset shows XRD θ-2θ scans for the PMN-PT(222) substrate under the corresponding remnant states. (b) and (c) The nonvolatile resistance switching of the SRO film by a sequence of pulse electric fields at $T=300$ K.

in Figs. 4(b) and 4(c). We note that a reset step by applying appropriate positive electric field pulses is required to set the polarization vectors to the fully downward direction with the minimum resistance, before writing to different higher resistances. This is to refresh the initial state to ensure that the finial state reached by every selective negative electric field pulse is reproducible.[17,20,26,27] Under such circumstances, our device allows to store nonvolatile information in the form of voltage-induced remnant strain states and read out the same information from the remnant resistance states in a nondestructive manner. The domain-engineered ferroelastic switching offers a promising approach for designing low power consuming nonvolatile memory devices.

In summary, we reported a comprehensive study of ferroelectric and ferroelastic domain switching-induced *in situ* lattice strain on the electronic transport properties in the SRO/PMN-PT(111) multiferroic heterostructures. The ferroelectric poling of the PMN-PT substrate enables the contraction of the film in-plane lattice, which, in turn, moderately manipulates the electronic transport of the SRO film through adjusting orbital hybridization between the Ru 4*d* orbitals and O 2*p* orbitals. The quantitative relationship between the resistance evolution ($\Delta R/R$) and the induced in-plane strain of the film can be analyzed using the converse piezoelectric effect. The multiple well-separated nonvolatile resistance states can be reversibly switched by precisely selecting the vertically applied voltage pulses, which is deeply associated with the ferroelastic domain switching-induced dissimilar in-plane strain states near the coercive field of the substrate. This work provides a framework for exploring electrically controlled nonvolatile tuning of lattice-coupled order parameters and delivering next-generation reconfigurable, energy efficient spintronic memory devices using domain engineering.

This work was supported by the National Key Project for Basic Research (Grant No. 2014CB921002), the National Natural Science Foundation of China (Grant Nos. 11374225, 11574227, and 11504432), Shandong Provincial Natural Science Foundation, China (BS2015DX002), and the Research Grant Council of Hong Kong (Project No. HKU 702112 P).

[1]D. Pantel, S. Goetze, D. Hesse, and M. Alexe, Nat. Mater. **11**, 289 (2012).
[2]R. O. Cherifi, V. Ivanovskaya, L. C. Phillips, A. Zobelli, I. C. Infante, E. Jacquet, V. Garcia, S. Fusil1, P. R. Briddon, N. Guiblin, A. Mougin, A. A. Ünal, F. Kronast, S. Valencia, B. Dkhil, A. Barthélémy, and M. Bibes, Nat. Mater. **13**, 345 (2014).
[3]C. A. F. Vaz, J. Hoffman, Y. Segal, J. W. Reiner, R. D. Grober, Z. Zhang, C. H. Ahn, and F. J. Walker, Phys. Rev. Lett. **104**, 127202 (2010).
[4]Y. Lee, Z. Q. Liu, J. T. Heron, J. D. Clarkson, J. Hong, C. Ko, M. D. Biegalski, U. Aschauer, S. L. Hsu, M. E. Nowakowski *et al.*, Nat. Commun. **6**, 5959 (2015).
[5]J. X. Shen, J. Z. Cong, Y. S. Chai, D. S. Shang, S. P. Shen, K. Zhai, Y. Tian, and Y. Sun, Phys. Rev. Appl. **6**, 021001 (2016).
[6]M. Liu, T. X. Nan, J. M. Hu, S. S. Zhao, Z. Y. Zhou, C. Y. Wang, Z. D. Jiang, W. Ren, Z. G. Ye, L. Q. Chen, and N. X. Sun, NPG Asia Mater. **8**, e316 (2016).
[7]C. Sow, A. K. Pramanik, and P. S. Anil Kumar, J. Appl. Phys. **116**, 194310 (2014).
[8]M. Zheng and W. Wang, ACS Appl. Mater. Interfaces **8**, 14012 (2016).
[9]X. W. Wang, Y. Q. Zhang, H. Meng, Z. J. Wang, D. Li, and Z. D. Zhang, J. Appl. Phys. **109**, 07D707 (2011).
[10]Z. Fang, N. Nagaosa, K. S. Takahashi, A. Asamitsu, R. Mathieu, T. Ogasawara, H. Yamada, M. Kawasaki, Y. Tokura, and K. Terakura, Science **302**, 92 (2003).
[11]G. Koster, L. Klein, W. Siemons, G. Rijnders, J. S. Dodge, C. B. Eom, D. H. A. Blank, and M. R. Beasley, Rev. Mod. Phys. **84**, 253 (2012).
[12]C. H. Ahn, R. H. Hammond, T. H. Geballe, M. R. Beasley, J.-M. Triscone, M. Decroux, Ø. Fischer, L. Antognazza, and K. Char, Appl. Phys. Lett. **70**, 206 (1997).
[13]C. H. Ahn, T. Tybell, L. Antognazza, K. Char, R. H. Hammond, M. R. Beasley, Ø. Fischer, and J.-M. Triscone, Science **276**, 1100 (1997).
[14]A. Herklotz, M. Kataja, K. Nenkov, M. D. Biegalski, H.-M. Christen, C. Deneke, L. Schultz, and K. Dörr, Phys. Rev. B **88**, 144412 (2013).
[15]W. P. Zhou, Q. Li, Y. Q. Xiong, Q. M. Zhang, D. H. Wang, Q. Q. Cao, L. Y. Lv, and Y. W. Du, Sci. Rep. **4**, 6991 (2014).
[16]S. Zhang, Y. G. Zhao, P. S. Li, J. J. Yang, S. Rizwan, J. X. Zhang, J. Seidel, T. L. Qu, Y. J. Yang, Z. L. Luo *et al.*, Phys. Rev. Lett. **108**, 137203 (2012).
[17]M. Liu, B. M. Howe, L. Grazulis, K. Mahalingam, T. X. Nan, N. X. Sun, and G. J. Brown, Adv. Mater. **25**, 4886 (2013).
[18]M. Liu, J. Hoffman, J. Wang, J. X. Zhang, B. Nelson-Cheeseman, and A. Bhattacharya, Sci. Rep. **3**, 1876 (2013).
[19]T. X. Nan, M. Liu, W. Ren, Z. G. Ye, and N. X. Sun, Sci. Rep. **4**, 5931 (2014).
[20]W. P. Zhou, Y. Q. Xiong, Z. M. Zhang, D. H. Wang, W. S. Tan, Q. Q. Cao, Z. H. Qian, and Y. W. Du, ACS Appl. Mater. Interfaces **8**, 5424 (2016).
[21]R. K. Zheng, Y. Jiang, Y. Wang, H. L. W. Chan, C. L. Choy, and H. S. Luo, Phys. Rev. B **79**, 174420 (2009).
[22]S. P. Timoshenko and J. N. Goodier, *Theory of Elasticity* (McGraw-Hill, New York, 1987), Chap. 2.
[23]R. K. Zheng, H.-U. Habermeier, H. L. W. Chan, C. L. Choy, and H. S. Luo, Phys. Rev. B **81**, 104427 (2010).
[24]A. Vailionis, W. Siemons, and G. Koster, Appl. Phys. Lett. **93**, 051909 (2008).
[25]W. L. Lu, K. H. He, W. D. Song, C. J. Sun, G. M. Chow, and J. S. Chen, J. Appl. Phys. **113**, 17E125 (2013).
[26]Y. J. Yang, Z. L. Luo, M. M. Yang, H. L. Huang, H. B. Wang, J. Bao, G. Q. Pan, C. Gao, Q. Hao, S. T. Wang, M. Jokubaitis, W. Z. Zhang, G. Xiao, Y. P. Yao, Y. K. Liu, and X. G. Li, Appl. Phys. Lett. **102**, 033501 (2013).
[27]B. W. Zhi, G. Y. Gao, H. R. Xu, F. Chen, X. L. Tan, P. F. Chen, L. F. Wang, and W. B. Wu, ACS Appl. Mater. Interfaces **6**, 4603 (2014).